JOURNAL OF MATERIALS SCIENCE 37 (2002) 2323–2329

# Microstructural characterization of magnesias derived from different sources and their influence on the structure of ceramic films formed on a 3% silicon steel surface

M. G. M. M. CESAR
*Acesita Research Center, Praça 1° de maio, 9, CEP 35180-000, Timóteo, MG, Brazil*
*E-mail: gracamelo@acesita.ind.br*

D. C. L. VASCONCELOS, W. L. VASCONCELOS
*Laboratory of Ceramic Materials, Department of Metallurgical and Materials Engineering, Federal University of Minas Gerais, R. Espírito Santo, 35, sala 206, CEP 30160-030, Belo Horizonte, MG, Brazil*
*E-mail: wlv@demet.ufmg.br*

A study on the influence of the type of magnesium oxide on the structure of the ceramic coating and consequently on the magnetic properties of a 3% Si steel was carried out. Decarburized samples coming from industrial equipment were coated with magnesia slurries and submitted to final annealing at 1200°C for 15 hours under $H_2$ atmosphere. We used magnesia synthesized from magnesium chloride and dolomite. The magnesia samples were characterized using granulometry measurements, scanning electron microscopy (SEM), nitrogen adsorption-desorption analyses, helium pycnometry, thermal analyses (TG and DTA), reactivity tests and calcination mass loss. The magnesia sintered from brine has the highest density, surface area and porosity. The rheological behavior of magnesia slurries, the magnetic properties of the steel and the ceramic film structure were correlated with the type of magnesia used. The slurry made with MgO from dolomite has the highest viscosity and the slurry made with oxide from brine the smallest one. Brine magnesia films are darker, thicker and rougher and sea water magnesia films are light gray, thinner and smoother. 

## 1. Introduction

The cores of electrical transformers and other types of electrical induction apparatus are made from steel sheets with soft magnetic properties. Such sheets are prepared by cold rolling the silicon-containing steel into sheet form, coiling the steel sheet into rolls and thereafter annealing the coiled steel by a controlled heat process to produce grain oriented structures with appopriate magnetic properties. During the annealing process in hydrogen atmosphere the large steel coils may fuse to itself in the absence of a suitable separating medium. Conventionally, the sticking of coils can be avoided by placing a thin coating of magnesium oxide on the steel surface prior to coiling. This coating will perform three different functions. The first one is to provide the separation of the various turns or layers of the coiled material to prevent sticking during high temperature annealing. A second function of the coating is to aid in the chemical purification of the steel. The third function of the coating is forming on the surface of the steel a ceramic coating which will provide electrical insulation between layers, which is required for its use as core in a transformer [1].

Usually, a 3% Si steel strip (breadth of 1000 mm) is coated with an aqueous slurry of magnesia which is dried at low heat and then the steel strip is wound up in coil-form and annealed at about 1200°C. During this annealing, a part of the magnesium oxide coating reacts with silica (previously formed during the step of steel decarburization) from the steel to form a forsterite ($Mg_2SiO_4$) film, according to the following reaction:

$$2MgO + SiO_2 \rightarrow Mg_2SiO_4. \quad (1)$$

The physical properties of the ceramic film are influenced by the magnesia composition and microstructure (surface area, porosity, density, reactivity).

In the presence of water, magnesium oxide hydrates to form magnesium hydroxide to a substantial degree. The presence of magnesium hydroxide in a magnesium oxide composition releases $H_2O$ which, unless removed before the annealing, can impair electrical properties of the dried and annealed steel coating. Excessive water present in the coating during the final annealing will usually produce a porous ceramic film which will not protect the steel and will not prevent oxide formation [2, 3].

Considerable work have been done to improve the properties of the insulating ceramic film by addition of chemical compounds ($TiO_2$, $MnO_2$, $Ca(H_2PO_4)_2$) to the MgO. It was further observed that phosphate addition made the ceramic film smoother, lighter grey and more resistant to oxidation [4–9].

The aim of this work is to evaluate the influence of magnesia sintered from brine, sea water and dolomite on the structure of the ceramic film formed on the surface of a 3% Si steel.

## 2. Experimental procedure

The substrates used in this work were samples (305 mm × 120 mm × 0.27 mm) obtained from a 3% Si steel decarburized coil. The coating slurries were prepared by mixing 900 g of deionized water and 150 g of MgO. 12% of calcium phosphates and 3.5% of colloidal silica based on the weight of the MgO were also added to the water. The MgO samples tested were obtained from sea water, brine and dolomite (Table I). The steel samples were coated with the slurries using rolls. The coated samples were then dried by heating them to a temperature sufficient to evaporate the water (furnace temperature = 300°C). The dried weight of the coating was 5 g/m$^2$. The coated stock was then subjected to a final high heat treatment at 1200°C for 15 h under hydrogen atmosphere.

The magnesia granulometry was measured using 74 $\mu$m and 44 $\mu$m ASTM standard sieves. The screen tests were carried out using 10 g of sample. The particle size distribution was determined by a laser diffraction particle sizer, Marlvern, Master Size S. The samples were added (200 milligrams) to anydrous ethanol and the measurements were made after 180 s of ultrasonic time.

The structures of magnesium oxide samples were characterized using scanning electron microscopy (SEM), nitrogen adsorption-desorption analyses (Autosorb 1, Quantachrome), helium pycnometry (multipycnometer, Quantachrome), thermogravimetry (TG) and differential thermal analyses (DTA) (TA50, Shimadzu), reactivity tests and calcination mass loss. The rheological behavior of magnesia slurries was measured with a Brookfield Viscometer, Model LVT, using NO. 1 Spindle at 60 rpm. The viscosity was recorded in centipoise, up to 6 minutes. The slurries were prepared by mixing 520 g of deionized water, 60 g or 75 g of MgO, 12% of phosphates and 3.5% of coloidal silica.

After the final heat treatment and cooling to room temperature, the excess of magnesium oxide was scrubbed from the surface of each coated sheet by brushing with a cotton clothe. The measurements of the steel magnetic properties were conducted under an alternating magnetic field of 1.7 T at 60 Hz by Epstein testing method (ASTM 725) with Brockhauss equipment.

The ceramic films of the samples (305 mm × 30 mm × 0.27 mm) were evaluated regarding electrical resistivity (Franklin test, ASTM 717), adherence (after bending by 180 degrees with a cilinder with 32 mm of diameter), morphology (thickness and roughness) and forsterite grain size (Leco Image Analysis).

The thickness of each ceramic film represents the average of 160 measurements made in 6 areas with about 81 $\mu$m length by surface. The relative roughness of the film with the base metal was evaluated considering equal 1 the roughness of a straight line. The estimation of the forsterite grain size was made by Heyn linear intercept (ASTM E 112), using a film surface image (10000 magnification) and a Leco Image Analysis (300 measurements were made).

TABLE I Kinds of magnesia

| MgO | | Source |
|---|---|---|
| A | Brine | ($MgCl_2$) |
| B | Sea water | ($MgCl_2$) |
| C | Dolomite | ($CaMg(CO_3)_2$) |

## 3. Results and discussion

### 3.1. Granulometry

The magnesia screen test results are shown in Table II. Fig. 1 is a graphic representation of the particle size distribution of each magnesia after 180 s of ultrasonic time used for dispersing the sample in the alcohol medium. Table III presents the corresponding results of $D_{50}$ and $D_{90}$. It can be noted that MgO A presents the thinnest granulometry in the sieve test and the lowest values of $D_{50}$ e $D_{90}$. MgO C is the coarsest and MgO B has an

TABLE II Sieve test results

| | % impassable through | | |
|---|---|---|---|
| ASTM sieve | MgO A | MgO B | MgO C |
| 74 $\mu$m (200 mesh) | 0 | 0.1 | 0.7 |
| 44 $\mu$m (325 mesh) | 0 | 0.3 | 1.5 |

TABLE III Results of $D_{50}$ e $D_{90}$

| Diameter | MgO A | MgO B | MgO C |
|---|---|---|---|
| $D_{50}$ | 2.0 $\mu$m | 4.1 $\mu$m | 6.4 $\mu$m |
| $D_{90}$ | 9.6 $\mu$m | 19.7 $\mu$m | 21.1 $\mu$m |

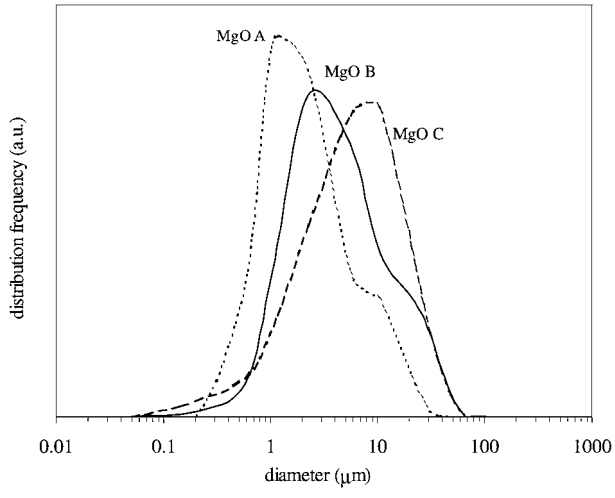


*Figure 1* Particle size distribution after 180 s ultrasonic.

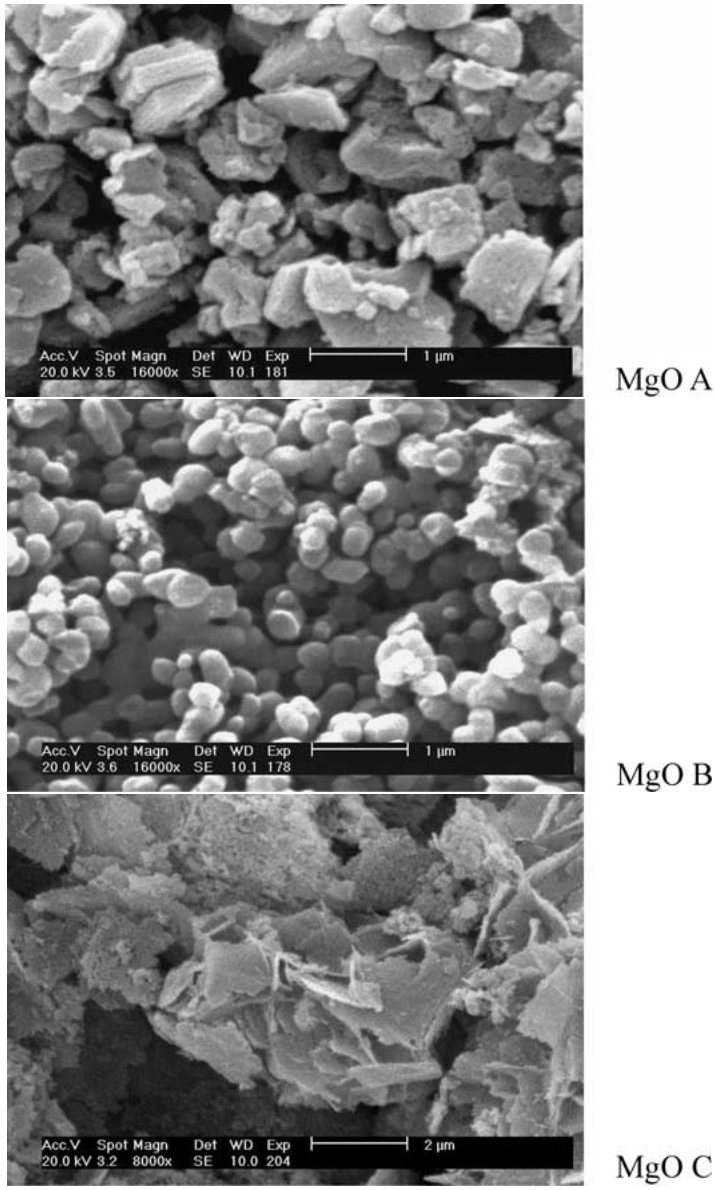


*Figure 2* SEM micrographs of agglomerates and primary particles of magnesia from different sources.

intermediate granulometry. The three types of magnesia have monomodal distribution, which is narrower for magnesia C.

### 3.2. Primary particles morphology (SEM)

The samples were analyzed using several magnifications to identify the agglomerates and the primary particles morphology (Fig. 2). MgO A shows small and disperse agglomerates, MgO B bigger, more rounded and compact ones and MgO C presents agglomerates less compact than MgO B, but with similar size. These results are coherent with the sieve and laser granulometry results ($D_{90}$).

The primary particles were analyzed using a magnification of 8000×. MgO A presents rombohedrical structure with maximum dimension of 0.90 $\mu$m. MgO B presents rounded primary particles with an average diameter around 0.4 $\mu$m, whereas MgO C has lamellar primary particles of about 2 $\mu$m. MgO A particles were easily observed as isolated particles, while the primary particles of magnesia B and C were observed in agglomerates. These results suggest that $D_{50}$ values of Table III refer to small agglomerates. The magnesias B and C with higher $D_{50}$ values show smaller primary particles, with round and lamellar shapes, which explain their strongest tendency to form stable agglomerates [6].

### 3.3. Nitrogen adsorption-desorption

Table IV presents the specific surface area, specific pores volume and average pore radius for each magnesia.

Magnesia A presents the largest surface area and has more and coarser pores than magnesias B and C. As shown in Fig. 3, the volume and size of the pores tend to increase as the surface area increases.

TABLE IV Pore structure parameters

| MgO | Specific surface area ($m^2$/g) | Specific pore volume ($cm^3$/g) | Average pore radius (nm) |
|---|---|---|---|
| A | $22.9 \pm 0.5$ | $0.199 \pm 0.033$ | $17.5 \pm 3.3$ |
| B | $17.1 \pm 0.4$ | $0.097 \pm 0.018$ | $11.4 \pm 2.3$ |
| C | $18.8 \pm 0.4$ | $0.127 \pm 0.010$ | $13.5 \pm 1.3$ |

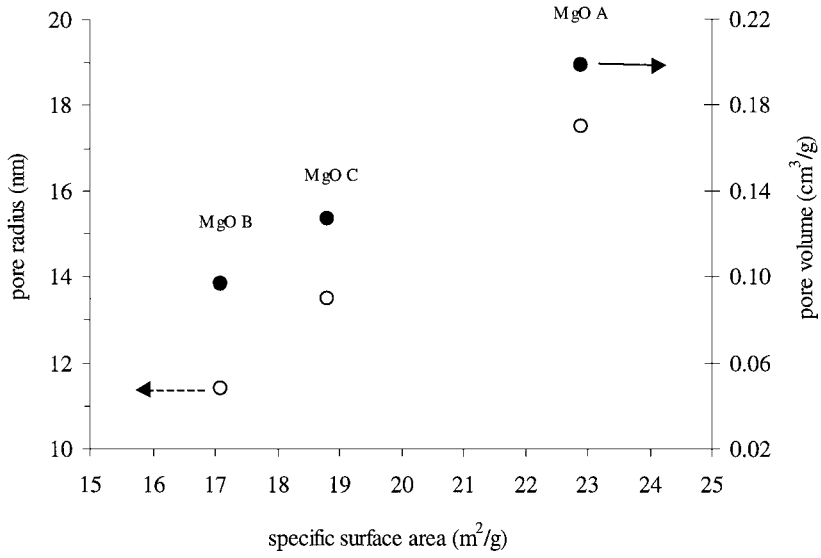


*Figure 3* Volume and radius of pores as function of surface area.

## 3.4. Helium pycnometry

Table V presents the mean apparent density of the solid part of magnesia particles. The data represent an average of 3 different evaluations; for each evaluation 12 tests were carried out.

Magnesia A presents higher density and the other two show similar results, slightly lower for MgO C. The higher density of MgO A may be related to a higher calcination temperature in the process of making the oxide [3].

## 3.5. Thermal analyses

The hydration of all reactive grades of magnesium oxides leads to the formation of magnesium hydroxide, $Mg(OH)_2$. The hydration rate of the various magnesium oxides may vary from a few hours, in the case of reactive oxides obtained at low temperature from a hydroxide or basic carbonate, to months or years for dead burned grades. Both magnesium hydroxide and magnesium oxide absorb moisture and carbon dioxide from the air. With sufficiently long exposure times, reactive grades of magnesium oxide are gradually converted into basic carbonate ($5MgO \cdot 4CO_2 \cdot xH_2O$) [3].

Thermal decomposition of magnesium hydroxide begins about 350°C (reaction 2), although much higher temperatures are required to drive off the last traces of water. The decomposition of carbonates begins around 450°C.

$$Mg(OH)_2 \rightarrow MgO + H_2O. \qquad (2)$$

Thermogravimetric analysis (TG) and differential thermal analysis (DTA) were carried out in order to characterize the physical chemical behavior of the different kinds of MgO. Table VI shows the main results, representing the average of 3 TG analyses and 2 DTA analyses for each sample. Figs 4 and 5 show the TG and DTA results for MgO B.

TABLE V Density of MgO particles

| MgO | Density (g/cm³) |
|---|---|
| A | 3.59 ± 0.01 |
| B | 3.38 ± 0.06 |
| C | 3.25 ± 0.05 |

TABLE VI TG and DTA results

| MgO | Weight loss (%) | Heat variation (J/g) |
|---|---|---|
| A | −1.6 | −165 |
| B | −2.3 | −190 |
| C | −1.8 | −255 |

The TG curves for all samples showed a weight loss upon heating to about 400°C, which is associated to the presence of adsorbed and chemically combined ($Mg(OH)_2$) water. The three kinds of magnesium oxide presented a low hydration (weight loss <3%) and no evidence of residual carbonates.

The DTA results confirm that part of the weight loss observed in the TG analysis is related to the endothermic decomposition reaction of the magnesium hydroxide at about 300°C.

## 3.6. Reactivity and loss on ignition

Citric acid activity (CAA), or reactivity, is a measure of the hydration rate of the magnesium oxide and is determined by measuring the time required for a given

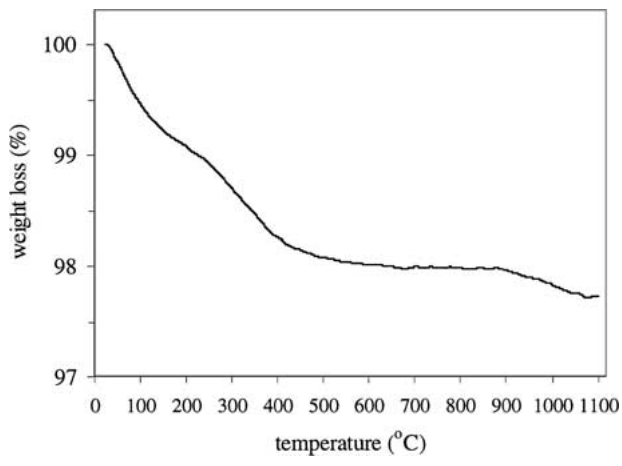


*Figure 4* TG curve of MgO B.

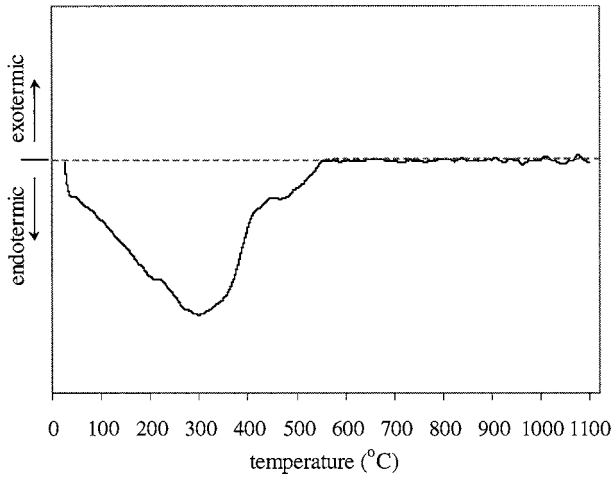


*Figure 5* DTA results of MgO B.

weight of magnesia to provide hydroxyl ions sufficient to neutralize a given weight of citric acid (reaction 3). It follows that a low CAA value represents a relative reactivity (active), i.e., the magnesia hydrates rapidly. Usually the rate of hydration is of greater significance than the eventual degree of hydration [11].

$$2H_6C_6H_6O_7 + 3MgO \rightarrow Mg_3(C_6H_6O_7)_2 + 6H_2O \quad (3)$$

The loss on ignition of magnesia is a measure of the degree of hydration of MgO, i.e., of the formation of $Mg(OH)_2$. The sample is heated at 1000°C, for one hour and is weighed before and after heat treatment [1].

Table VII shows the CAA and ignition loss results of each magnesia. The CAA results are very similar in the range of 60 s to 63 s. The ignition loss results were lower than 2% and MgO B presents a slightly higher value. These ignition loss values are in good agreement with TG results.

## 3.7. Slurry viscosity

Magnesium oxide suspension (slurry) used for coating silicon steel is generally kept at a viscosity which allows the oxide particles to remain in suspension and which is suitable for coating.

Fig. 6 shows the viscosity as function of time for slurries prepared with 11% and 14% of magnesium oxide. MgO C slurries present the highest viscosity values and MgO A slurry the lowest one. All the slurries present a decrease of viscosity in time, which we relate to a partial sedimentation of MgO during the test [5, 8].

It has been found that viscosity depends on granulometry, reactivity and concentration of MgO. The highly reactive magnesium oxide tends to hydrate and the formation of hydroxide increases the viscosity [8, 11].

The three kinds of MgO studied have similar reactivity in the CAA test and the differences in the particle

TABLE VII CAA and ignition loss results

| MgO | CAA (s) | Ignition loss (%) |
|---|---|---|
| A | 60 | 1.1 |
| B | 63 | 1.5 |
| C | 60 | 1.3 |

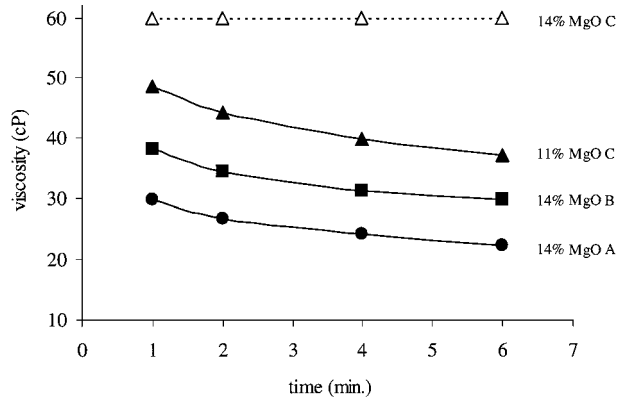


*Figure 6* Slurry viscosity as function of time.

size distribution or granulometry do not explain the results of the viscosity. One hypothesis to be considered is that the highest viscosity of the MgO C slurry is related to a higher hydration of the oxide after slurry preparation [5, 8].

For the coating of the steel samples in laboratory, all the slurries were prepared with 14% MgO and adjustments of speed and pressure were made on the roll coater in order to compensate the different viscosities of the slurries and to get the magnesia coating weight at about 5 g/m$^2$ on each surface of the steel sheet.

## 3.8. Magnetic properties

Table VIII shows the core loss (W/kg) for each magnesia used in this work. Each result corresponds to Epstein test of 20 strips of 305 mm × 30 mm. To evaluate the repeatability of the experiment, two slurries were prepared with MgO B and 40 samples were coated.

The core loss and induction results were very close and the magnetic properties variability with the kind of MgO was lower than that obtained with the individual Epstein set from the oxide B (B and B′).

## 3.9. Structure of the forsterite film

Table IX, Figs 7 and 8 present results on the color, morphology (thickness and roughness and the average grain

TABLE VIII Magnetic properties - Epstein test

| MgO | Epstein set | Core loss (1.7 T/60 Hz for 0.25 mm thickness) (W/kg) | Induction (800 A/m) (T) |
|---|---|---|---|
| A | A | 1.448 | 1.849 |
| | B | 1.408 | 1.857 |
| B | | | |
| | B′ | 1.464 | 1.846 |
| C | C | 1.434 | 1.849 |

TABLE IX Forsterite ceramic film

| | | Forsterite film morphology | | |
|---|---|---|---|---|
| MgO | Appearance of a film surface | Thickness average ($\mu$m) | Relative roughness | Average forsterite grain diameter ($\mu$m) |
| A | Dark gray color | $1.52 \pm 0.43$ | 1.095 | $0.54 \pm 0.27$ |
| B | Light gray color | $1.23 \pm 0.31$ | 1.067 | $0.44 \pm 0.18$ |
| C | Medium gray color | $1.42 \pm 0.39$ | 1.090 | $0.48 \pm 0.22$ |

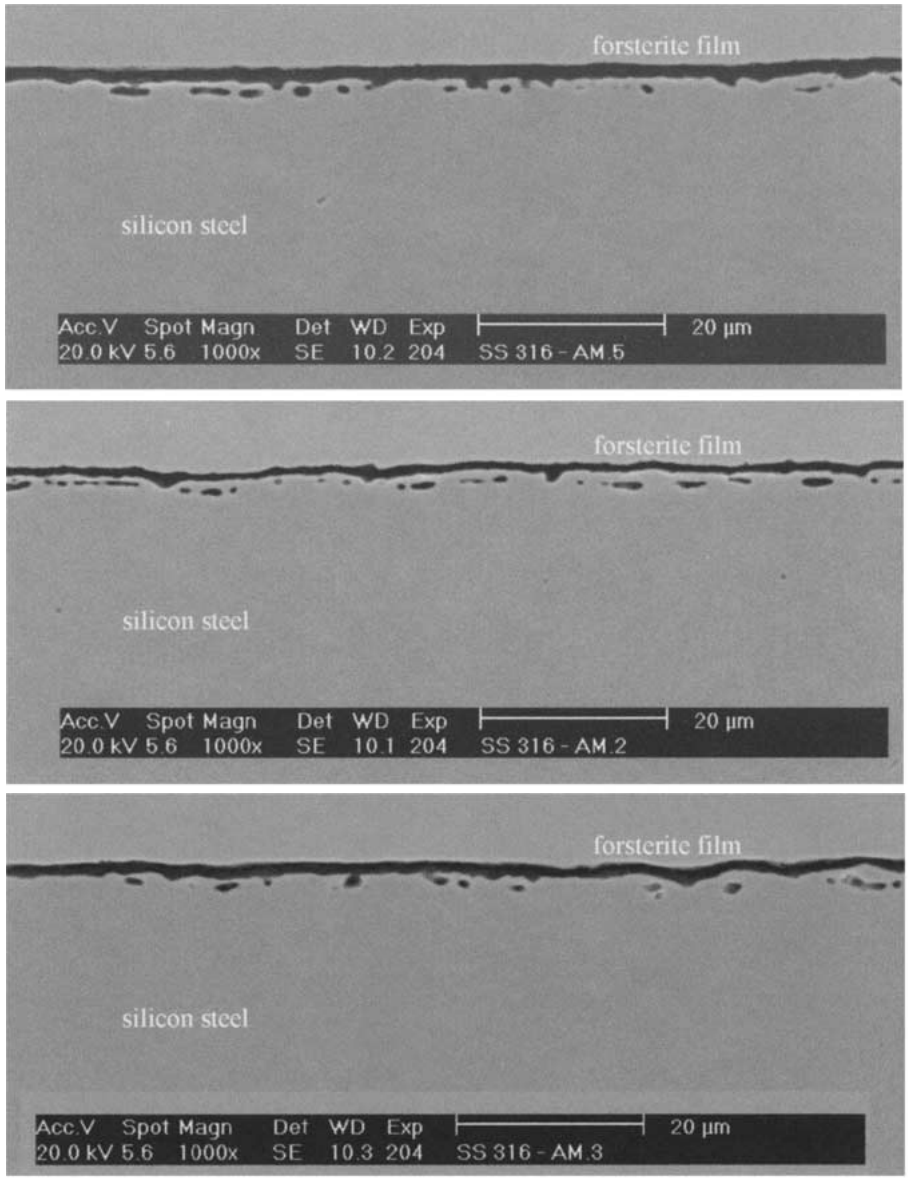


*Figure 7* Phomicrographs of the cross-section of the forsterite film.

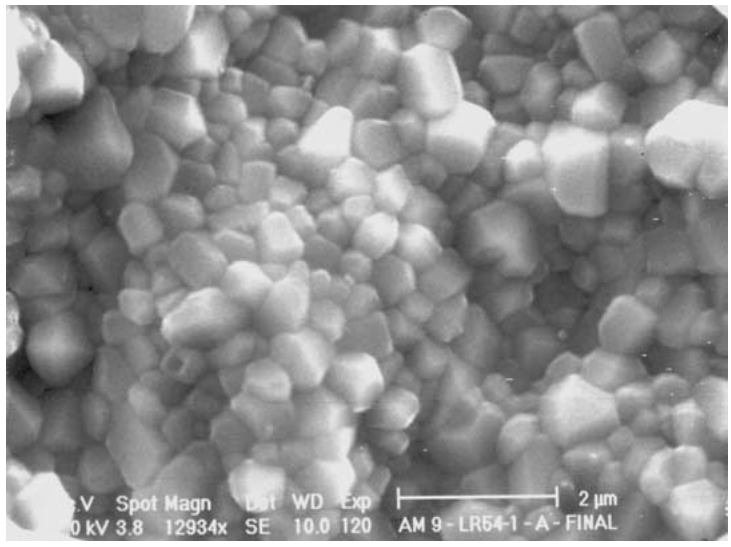


*Figure 8* Grain structure of the forsterite film obtained with MgO A.

size of forsterite for each magnesia. The film obtained with MgO A is darker and rougher than the others and has a higher thickness. On the other hand, the film obtained with MgO B has the lightest color and is the smoothest and thinnest. It has been known that the dark gray color is related to a thick and rough film.

We observed that the forsterite film structure can be related to the microstructure of the MgO particles. The

thicker and rougher film can be associated to a magnesia with higher pores volume and size of pores and the thinner and smoother film to a magnesia with smaller pores volume and smaller surface area, i.e. MgO A and B, respectively.

The electrical resistivity of the forsterite films obtained with the magnesia A, B and C ranges between 3 $\Omega \cdot cm^2$ and 4 $\Omega \cdot cm^2$, which is a typical range for a continuous film, and the adhesion of the films was also good. The good adherence results can be related to the small average grain size of the forsterite crystals, which are smaller than 0.7 $\mu$m [12].

## 4. Conclusions

The morphology of the magnesia particles varies significantly with the raw material and with the process used to obtain the oxide. The oxide particles sintered from magnesium chlorides have rombohedrical or spheroidal structure if they come from brine or sea water. The oxide particles sintered from dolomite present lamellar structure. The magnesia sintered from brine has the highest density, surface area and porosity. The three kinds of MgO present different particle size distribution. The brine magnesia is the thinnest and has the smallest agglomerates and the dolomite magnesia is the coarsest and has the biggest agglomerates.

The three kinds of MgO present different rheological behavior. The slurry made with MgO from dolomite has the highest viscosity and the slurry made with oxide from brine the smallest one. This result can be associated with the different hydration behavior of each oxide in the water.

The kind of magnesia affects the morphology of the ceramic film: color, thickness and roughness. Brine magnesia films are darker, thicker and rougher and sea water magnesia films are light gray, thinner and smoother. These results are associated with the pore structure of each kind of magnesia.

## References


1. J. F. STEGER *et al.*, Int. Cl. C22c39/46 U.S.P. no. 3,841,925. 15 Oct. 1974.
2. W. S. SOPP, Calgon Corporation, USA, Int. Cl. C01F 5/06. U.S.P. no. 4,443,425. 17 April 1984.
3. J. W. MEELOR, in "A Comprehensive Treatise and Theoretical Chemistry" (Longmans, London, 1952).
4. H. SHIMANAKA, Kawasaki Steel Corporation, Japan, Int. Cl. H01F14. U.S.P. no. 4,113,530. 12 Sep. 1978.
5. D. C. L. VASCONCELOS, Master Thesis, Federal University of Minas Gerais, Belo Horizonte, Brazil, 1998.
6. M. G. M. M. CESAR and I. N. GONÇALVES, *Acta Microscopica* **7A** (1998) 29.
7. D. C. L. VASCONCELOS, M. G. M. M. CESAR and W. L. VASCONCELOS, *ibid.* **7A** (1998) 457.
8. *Idem.*, in Proceedings of the 13rd Brazilian Congress of Materials Science and Engineering, Cuitiba, PR, Brazil, December 1998, p. 1840.
9. D. C. L. VASCONCELOS, M. G. M. M. CESAR, M. A. CUNHA and W. L. VASCONCELOS, *Materials Research* **2** (1999) 159.
10. D. C. L. VASCONCELOS, M. G. M. M. CESAR and W. L. VASCONCELOS, *Cerâmica* **46** (2000) 239.
11. M. H. HASELKORN, Int. Cl. H01F/04, U.S.P. no. 4,160,189. 18 Sept. 1979.
12. T. ICHIDA *et al.*, Int. Cl. H01F/04, U.S.P. no. 4,190, 469. 26 Feb. 1980.



*Received 17 April*
*and accepted 29 November 2001*